J. Fluid Mech. (2012), *vol.* 691, *pp.* 440–460.
doi:10.1017/jfm.2011.482

Nonlinear landslide tsunami run-up

M. Sinan Özeren and Nazmi Postacioglu†

Istanbul Technical University, 34469, Maslak, Istanbul, Turkey

(Received 12 April 2010; revised 17 October 2011; accepted 31 October 2011;
first published online 13 December 2011)

Inhomogeneous nonlinear shallow-water equations are studied using the Carrier–Greenspan approach and the resulting equations are solved analytically. The Carrier–Greenspan transformations are commonly used hodograph transformations that transform the nonlinear shallow-water equations into a set of linear equations in which partial derivatives with respect to two auxiliary variables appear. Yet, when the resulting initial-value problem is treated analytically through the use of Green's functions, the partial derivatives of the Green's functions have non-integrable singularities. This has forced researchers to numerically differentiate the convolutions of the Green's functions. In this work we remedy this problem by differentiating the initial condition rather than the Green's function itself; we also perform a change of variables that renders the entire problem more easily treatable. This particular Green's function approach is especially useful to treat sources that are extended in time; we therefore apply it to model the run-down and run-up of the tsunami waves triggered by submarine landslides. Another advantage of the method presented is that the parametrization of the landslide using sources is done within the integral algorithm that is used for the rest of the problem instead of treating the landslide-generated wave as a separate incident wave. The method proves to be more accurate than the techniques based on Bessel function expansions if the sources are very localized.

Key words: surface gravity waves, topographic effects

1. Introduction

Underwater landslides have the potential of creating tsunami waves that can locally become high enough to pose danger to coastal communities (Geist 2000; Ward 2001; Bardet *et al.* 2003; Watts *et al.* 2003; Geist, Lynett & Chaytor 2009; Özeren *et al.* 2010). In most cases underwater landslides occur in the shelf break offshore. In other cases such landslides may take place at a short distance from the shore such as the 1979 Nice Airport event (Assier-Rzadkiewicz *et al.* 2000) which was a human-created landslide tsunami, triggered during the landfilling activities in the airport complex. The run-down and run-up processes are the immediate practical consequences of these phenomena and in some cases analytical and semi-analytical approaches can shed some light on their physics. Carrier–Greenspan transformations (hereafter CG) have long been used to study shallow-water equations (Carrier & Greenspan 1958). More recently, there have been a number of studies that have applied the CG transformations to tsunami run-up problems. Tinti & Tonini (2005) used this approach to look at

† Email address for correspondence: nposta@hotmail.com

the run-up problem of conventional tsunamis, namely the tsunamis generated by the sudden vertical motion of the sea floor. In their analysis they find exact solutions for some particular initial conditions which we will show in, appendix A, to be related to Legendre functions with complex arguments. Carrier, Wu & Yeh (2003) calculated the Green's function composed of elliptic functions for the initial-value problem and they applied their development to both the problems of the initial waveforms with zero velocity and of incident waves of various shapes. It is worthwhile to note that the incident wave problems involve high-order derivatives of the convolution of the Green's function (equation (27) in Carrier *et al.* 2003). Kanoglu (2004) also looked at the run-up evolution of the initial waveforms (such as the Gaussian and N-waves) given with zero-velocity initial condition, adopting an approach based on Fourier–Bessel transformations. Kanoglu & Synolakis (2006), on the other hand, considered cases in which the initial incident wave has a finite amplitude. In this case, because of non-vanishing initial velocity, it is difficult to formulate an initial-value problem in the transformed space. Pritchard & Dickinson (2007) looked at the problem of run-up produced by sudden, localized uplift of the seabed and they obtained asymptotic approximations for the run-up. More recently Madsen & Schäffer (2010) used a variant of the CG approach to study the run-up evolution of N-waves which start their motion at a flat-bottomed offshore location. Our representation of Green's function will also yield relatively simple expressions for the run-down and run-up. Liu, Lynett & Synolakis (2003) studied the linearized landslide tsunami run-up problem without making the use of CG transforms. Instead they obtained a Bessel equation describing the waves using a change of variables. They obtained an analytical solution for the case in which the sliding velocity is equal to the velocity of the progressive waves. Assuming that the landslide starts from the shoreline and neglecting all the energy losses, this equality will be satisfied if the density of sliding material is twice that of the water. Their analytical solution has the advantage of not involving Green's functions and related convolutions. More recently Sammarco & Renzi (2008) investigated the linear waves excited by a landslide of finite width. Their method consists of expanding the tsunami source in terms of Laguerre polynomials. This technique allows them to catch the edge waves with relatively minor computational effort within a linear context.

Postacioglu & Özeren (2008) computed the dispersive waves produced by a block sliding down a hyperbolic-tangent profile using a semi-spectral method. Although their model was not designed to look at the edge waves in particular, when the landslide was assumed to move at a constant velocity, the Fourier transform of the free-surface deformation presented sharp peaks (figure 15 of Postacioglu & Özeren 2008). These are probably multiple reflections or edge waves. In this work, our motivation is to develop a new approach that would enable us to attack the run-up problem of tsunamis triggered by submarine landslides within the framework of CG transformations. Submarine mass failures usually occur as a result of triggering by large earthquakes. The slope angle, sediment characteristics, pore pressure and Coulomb friction coefficient for the interface between the sliding material and the basement rock are some of the main characteristics that determine the mechanics of these events that can potentially be very hazardous. Wang, Liu & Mei (2011) recently provided a semi-analytical solutions for submarine-generated tsunamis in which they examined the viscous and solid friction in detail. Submarine landslides may occur in places far from the shoreline and the energy losses of the slide, because of friction,

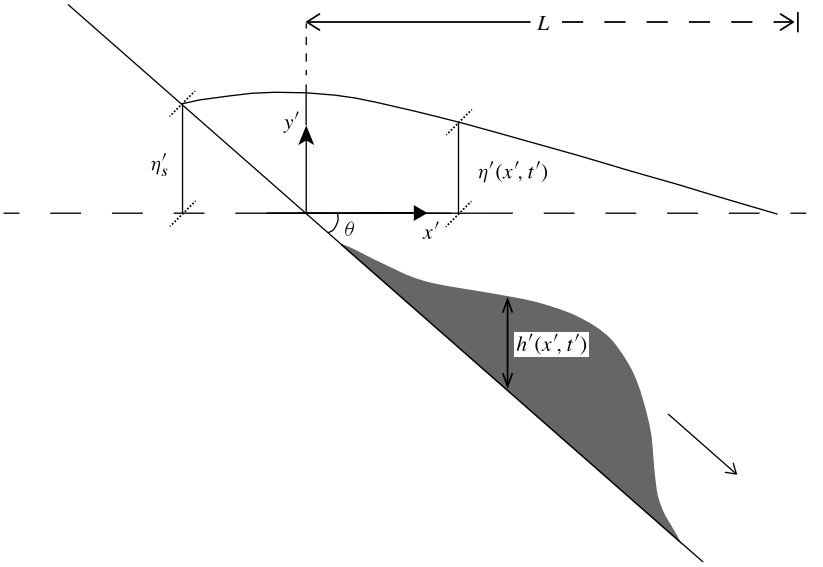

FIGURE 1. The non-dimensionalized geometry of the run-down and run-up problem of landslide tsunamis. The grey mass moving downwards represents the underwater landslide. Note that its shape and also the shape of the free surface are symbolic. Symbol α in (2.3) is equal to $\tan\theta$.

may lead to a variety of trajectory histories, hence we require our algorithm to resolve all such cases.

2. Formulation of the problem

2.1. *Governing equations*

The forced nonlinear shallow-water equations for a uniform slope can be written in dimensionless form as

$$[u(x+\eta-h)]_x+\eta_t=h_t, \tag{2.1}$$

$$u_t+uu_x+\eta_x=0, \tag{2.2}$$

where the subscripts represent partial derivatives and the unprimed quantities defined by

$$x=x'/L, \quad \eta=\eta'/L\alpha, \tag{2.3}$$

$$h=h'(t',x')/L\alpha, \quad t=\sqrt{\alpha g/L}t', \quad u=u'/\sqrt{g\alpha L} \tag{2.4}$$

are dimensionless. The dimensional quantities L, x', t', u' and g are a length scale, distance from the shoreline, the time, the velocity and the acceleration due to gravity respectively. A good choice for the length scale L may be the length of the sliding block. The dimensionless quantities η, u, h, α, t are the vertical displacement of the free surface, the depth-averaged horizontal velocity, the disturbance to the sea bottom due to the landslide activity, the slope, and the time respectively (see figure 1 for the dimensional geometry of the problem). The depth at a distance x' from the shoreline is thus given by $\alpha x'-h'(t',x')$. It is also assumed that $\alpha x'\gg h'$. In (2.1) the forcing term h_t represents the rate of change in the bathymetry because of the landslide activity.

2.2. *The CG transformation and the integral approach*

A hodograph transformation introduced by Carrier & Greenspan (1958) uses two distorted coordinates λ, σ and they are defined as

$$\lambda = t - u, \quad \sigma^2 = q = x + \eta, \quad u = -\varphi_\sigma/2\sigma, \quad \eta = \varphi_\lambda - \varphi_\sigma^2/8\sigma^2. \tag{2.5}$$

These are used to obtain a linearized set of equations; this is the CG transformation mentioned in the introduction. If we use the short-hand notation $\psi = \eta + (1/2)u^2$, our forced equations (2.1) and (2.2) would become

$$\psi_{\lambda\lambda} - \frac{1}{4}\left(\psi_{\sigma\sigma} + \frac{1}{\sigma}\psi_\sigma\right) \approx \left(J\frac{\partial h}{\partial t}\right)_\lambda \tag{2.6}$$

where $J = x_q t_\lambda - x_\lambda t_q$ is the Jacobian. Note that when obtaining (2.6) we have also neglected the $(uh)_x$ term on the left-hand side of (2.1) as the existence of the block would automatically violate the constant-slope assumption of the CG approach. For a block whose thickness is small compared to the water depth at the initial position of the sliding motion the $(uh)_x$ term is even less important than the $(v_b h)_x$ term, where v_b is the velocity of the sliding block. In any case, the analytical technique presented here is not capable of taking this term into account. Note that the velocity of the sliding block is implicitly included on the right-hand side of (2.6).

Equation (2.6) is not strictly linear. This is because of the presence of the Jacobian on the right-hand side and also because of the fact that h is, in general, a function of both x and t. In the context of the CG transformation x and t are not linear functions of ψ. However this particular nonlinearity, as we will show, is not a major factor for submarine landslides (it may possibly play an important role in waves created by subaerial landslides that splash onto the water surface; this issue, however, is beyond the scope of this paper). If we integrate (2.6) with respect to λ we obtain

$$\varphi_{\lambda\lambda} - \frac{1}{4\sigma}\varphi_\sigma - \frac{\varphi_{\sigma\sigma}}{4} \approx J\partial_t h \tag{2.7}$$

where, following Carrier *et al.* (2003), we use the short-hand $\psi = \varphi_\lambda$. For simplicity we will use an equals sign rather than $\approx$ for the further treatments arising from (2.6) and (2.7).

Let us start our discussion with the homogeneous form of (2.7). Tinti & Tonini (2005) discussed this equation and obtained, after lengthy derivations, exact analytical solutions for particular initial conditions with vanishing initial fluid velocity u (see their equations (3.26) and (3.27)). We will show in appendix A that their solution is directly expressible in terms of Legendre polynomials.

Carrier *et al.* (2003) found a Green's function for the equation (2.7), but the partial derivatives of this Green's function with respect to σ and λ had non-integrable singularities. Their strategy to surmount this difficulty was to convolve the Green's function with the driving force and then numerically differentiate these integral convolutions which are more regular than the Green's function itself. Kanoglu & Synolakis (2006) have the same formulation of the Green's function given by

$$G(\tilde{\sigma}, \sigma, \lambda - \tilde{\lambda}) = 2\tilde{\sigma}\int_0^\infty J_0(\omega\tilde{\sigma})J_0(\omega\sigma)\sin\left(\tfrac{1}{2}\omega(\lambda - \tilde{\lambda})\right)\,\mathrm{d}\omega \tag{2.8}$$

where $\tilde{\lambda}$ is the 'instant' of excitation and J_0 is the Bessel function of the first kind and order zero. The partial derivatives of this Green's function are singular but truncating the upper limit to a finite ω removes this singularity and, as long as

the initial condition does not contain high-frequency features in its Fourier spectrum, that does not lead to a significant loss of accuracy. For initial conditions containing discontinuities however, this practice may present problems because the Bessel functions, being continuous functions, are not suitable to approximate discontinuous functions. For the derivatives of discontinuous functions the situation is even worse.

When a localized disturbance acts on the bottom slope, the resulting perturbation on the water surface spreads out with a finite velocity. Therefore at any given time there is a sharp boundary between the affected and unaffected zones. In our formulation this sharp wavefront is reproduced precisely, with the wave vanishing outside the affected zone. The solution by Carrier *et al.* (2003) also has this property but, as mentioned earlier, the derivative of their Green's function has non-integrable singularities forcing them to numerically differentiate the convolutions with the Green's functions. The Bessel-function-based approach of Kanoglu & Synolakis (2006) on the other hand yields discontinuous integrals around the sharp wavefront. Numerical evaluations of such integrals often yield spurious oscillations around the wavefront.

Equation (2.7) corresponds to the forced wave equation on the plane with axial symmetry. To exploit this fact, we consider the more general problem of forced waves in the plane. The sources will be placed in such a way that the resulting wave field will have axial symmetry. The Green's function of the general problem then satisfies

$$\left(\frac{\partial^2}{\partial\lambda^2}-\frac{1}{4}\left(\frac{\partial^2}{\partial x^2}+\frac{\partial^2}{\partial y^2}\right)\right)G=\delta(\lambda-\tilde{\lambda})\delta(x-\tilde{x})\delta(y-\tilde{y}). \tag{2.9}$$

According to Witham (1974), p. 235, the related retarded Green's function is given as

$$G=\frac{1}{\pi\sqrt{(\lambda-\tilde{\lambda})^2/4-((x-\tilde{x})^2+(y-\tilde{y})^2)}} \tag{2.10}$$

but $G\equiv 0$ for $\lambda<\tilde{\lambda}$ or $((x-\tilde{x})^2+(y-\tilde{y})^2)>(\lambda-\tilde{\lambda})^2/4$.

Here the variables with tildes denote the position of the source. Since (2.7) represents an inhomogeneous wave equation with axial symmetry, an axisymmetrical distribution of sources in the x, y plane will lead to the solution of (2.7). Placing the sources on the perimeter of the circle with radius $\tilde{\sigma}=\sqrt{\tilde{x}^2+\tilde{y}^2}$, the Green's function becomes

$$G=\frac{1}{\pi}\int\frac{\mathrm{d}\phi}{\sqrt{(\lambda-\tilde{\lambda})^2/4-(\tilde{\sigma}^2+\sigma^2-2\sigma\tilde{\sigma}\cos\phi)}} \tag{2.11}$$

where the integral is evaluated within the sub-domain in which $(\lambda-\tilde{\lambda})^2/4-(\tilde{\sigma}^2+\sigma^2-2\sigma\tilde{\sigma}\cos\phi)\geqslant 0$. It is important to point out that $\sqrt{\tilde{\sigma}^2+\sigma^2-2\sigma\tilde{\sigma}\cos\phi}$ is the distance between the source $(\tilde{x},\tilde{y})$ and the target (x, y) in this Green's function formalism. If $(\lambda-\tilde{\lambda})^2/4-(\tilde{\sigma}^2+\sigma^2-2\sigma\tilde{\sigma}\cos\phi)$ is negative, then the wave excited at the instant $\tilde{\lambda}$ has not yet reached the point (x, y). The integral given by (2.11) is exactly equal to the Green's function exploited by Carrier *et al.* (2003) (see their equation (22)).

Now let us go back to the original equation we are trying to solve (equation (2.7)). If we rewrite this equation, this time by denoting its right-hand side simply as $S(\sigma,\lambda)$:

$$\varphi_{\lambda\lambda}-\frac{1}{4\sigma}\varphi_\sigma-\frac{\varphi_{\sigma\sigma}}{4}=S(\sigma,\lambda), \tag{2.12}$$

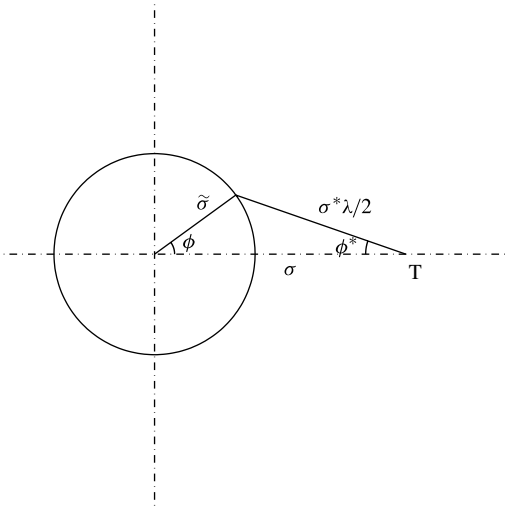

FIGURE 2. The geometrical setting to evaluate the integral given in (2.14). The sources are placed on the perimeter of the circle and the target point at which the field is evaluated is marked T.

the solution of this equation is given by

$$\varphi = \frac{1}{\pi}\int_0^{\lambda} \mathrm{d}\tilde{\lambda} \int_0^{\infty} \mathrm{d}\tilde{\sigma} \int \mathrm{d}\phi \frac{\tilde{\sigma} S(\tilde{\sigma}, \tilde{\lambda})}{\sqrt{(\lambda - \tilde{\lambda})^2/4 - (\tilde{\sigma}^2 + \sigma^2 - 2\sigma\tilde{\sigma}\cos\phi)}} \tag{2.13}$$

where the ϕ integral is evaluated within the same domain as the integral given in (2.11). When $|\sigma - \tilde{\sigma}| < (\lambda - \tilde{\lambda})/2 < |\sigma + \tilde{\sigma}|$ we can always find a critical angle ϕ_c that satisfies $(\lambda - \tilde{\lambda})^2/4 - (\tilde{\sigma}^2 + \sigma^2 - 2\sigma\tilde{\sigma}\cos\phi_c) = 0$. Consequently, the integration over ϕ is evaluated between ϕ_c and $2\pi - \phi_c$; this applies to all ϕ-integrals in the rest of the paper. If we now make a change of variable given by $\sigma^* = 2\sqrt{\tilde{\sigma}^2 + \sigma^2 - 2\tilde{\sigma}\sigma\cos\phi}/(\lambda - \tilde{\lambda})$, and $\phi^* = \cos^{-1}((\sigma - \tilde{\sigma}\cos(\phi))/(\sigma^*(\lambda - \tilde{\lambda})/2))$ (see figure 2 for definition of ϕ^*) equation (2.13) becomes

$$\varphi = \frac{1}{2\pi}\int_0^{\lambda} \mathrm{d}\tilde{\lambda}(\lambda - \tilde{\lambda}) \int_0^{1} \mathrm{d}\sigma^* \int_0^{2\pi} \mathrm{d}\phi^* \times \frac{\sigma^* S(\sqrt{\sigma^2 + (\lambda - \tilde{\lambda})^2(\sigma^*)^2/4 - \sigma\sigma^*(\lambda - \tilde{\lambda})\cos\phi^*}, \tilde{\lambda})}{\sqrt{1 - (\sigma^*)^2}}. \tag{2.14}$$

The integrals in the expression (2.14) are treated numerically. One interesting feature of the σ^* integral with integrable singularity $\sqrt{1 - (\sigma^*)^2}$ in particular is that it can be carried out using orthogonal polynomials in the interval [0,1] with a weight function containing the singular term (Amparo, Segura & Temme 2007, p. 132). In appendix C we give a detailed account of the numerics. It is important to note here that S is a function of both position and time, yet after the CG transformation, the dependence on the position becomes essentially the dependence on $(\sigma^*)^2$; therefore when differentiating φ defined in (2.14) with respect to σ, no singularities arise. This formulation can be used for various phenomena including conventional tsunamis (those created directly by the sudden uplift of the sea floor) in which case the source term S

becomes a Dirac's delta function in time, i.e. $S(\tilde{\sigma}, \tilde{\lambda}) = \delta(\tilde{\lambda})h(\tilde{\sigma})$, so (2.14) becomes

$$\varphi = \frac{\lambda}{2\pi}\int_0^1 \mathrm{d}\sigma^* \int_0^{2\pi} \mathrm{d}\phi^* \frac{\sigma^* h(\sqrt{\sigma^2 + \lambda^2 (\sigma^*)^2/4 - \sigma\sigma^*\lambda\cos\phi^*}, \tilde{\lambda} = 0)}{\sqrt{1-(\sigma^*)^2}} \tag{2.15}$$

where the integration with respect to $\tilde{\lambda}$ no longer occurs. Notice also that for $\lambda = 0$, φ takes zero value with the physical consequence of $u = -\varphi_\sigma/2\sigma$ becoming uniformly zero.

In the coastal region $\sigma \to 0^+$ the integrand in (2.15) may be expanded in power series of σ and carrying out the integration with respect to ϕ^*, one has

$$\varphi = \lambda \int_0^1 \mathrm{d}\sigma^*\sigma^* \frac{h + (\sigma^2/(2\sigma^*\lambda))h' + (\sigma^2/4)h''}{\sqrt{1-(\sigma^*)^2}} \tag{2.16}$$

where h' and h'' are given by

$$h' = \frac{\mathrm{d}h(\lambda\sigma^*/2)}{\mathrm{d}(\lambda\sigma^*/2)} \tag{2.17}$$

and

$$h'' = \frac{\mathrm{d}^2 h(\lambda\sigma^*/2)}{\mathrm{d}\,(\lambda\sigma^*/2)^2}. \tag{2.18}$$

The same expansion can be applied to (2.14) to yield

$$\varphi = \int_0^\lambda \mathrm{d}\tilde{\lambda}(\lambda - \tilde{\lambda}) \int_0^1 \mathrm{d}\sigma^*\sigma^* \frac{S + (\sigma^2/(2\sigma^*(\lambda - \tilde{\lambda})))S' + (\sigma^2/4)S''}{\sqrt{1-(\sigma^*)^2}} \tag{2.19}$$

where S, S', S'' are the source $S((\lambda - \tilde{\lambda})\sigma^*/2, \tilde{\lambda})$ and its first and second derivatives with respect to the first argument $(\lambda - \tilde{\lambda})\sigma^*/2$. An expansion up to second order is sufficient to evaluate run-down and run-up.

Now let us look at the complementary problem (we can also call this the *second* problem) in which the initial value of φ is different from zero but φ_λ is initially zero. The physical meaning of this is that the water surface is initially completely undisturbed but the initial fluid velocities are non-zero. The problem of the incident wave is a linear combination of these two complementary problems. To solve the second problem we introduce an intermediate variable $\tilde{\varphi}$ such that $\varphi = \partial_\lambda\tilde{\varphi}$. We then have

$$\tilde{\varphi} = \frac{\lambda}{2\pi}\int_0^1 \mathrm{d}\sigma^* \int_0^{2\pi} \mathrm{d}\phi^* \frac{\sigma^*\varphi(\gamma, \tilde{\lambda} = 0)}{\sqrt{1-\sigma^{*2}}} \tag{2.20}$$

where γ is given by

$$\gamma = \sqrt{\sigma^2 + \lambda^2\sigma^{*2}/4 - \sigma\sigma^*\lambda\cos\phi'}. \tag{2.21}$$

Note that the values of $\tilde{\varphi}$ and $\tilde{\varphi}_{\lambda\lambda}$ are both zero at $\lambda = 0$ (the latter is so because $\tilde{\varphi}$ and all its derivatives with respect to σ are zero initially and since $\tilde{\varphi}$ satisfies the wave equation in cylindrical coordinates, $\tilde{\varphi}_{\lambda\lambda}$ must also be zero initially).

It is worth noting that when the line $(t = 0, x : 0 \to \infty)$ in the physical space is mapped onto the (σ, λ) space using CG transformation, a curve, not a line, is obtained if the initial velocity is non-zero. Kanoglu & Synolakis (2006), for the first time, used

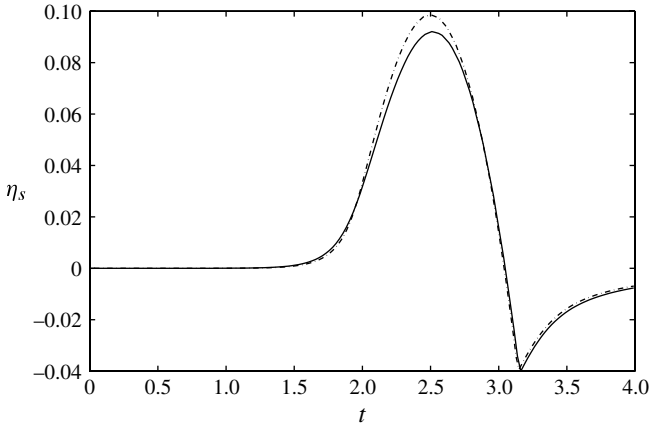

FIGURE 3. Shoreline motion η_s as function of non-dimensional time (the displacement of the shoreline is also non-dimensional). We carry out the calculation for an incident wave with the initial shape given by $\eta = a\exp(-k\,(x-x_0)^2)$ where $a = 0.017$, $x_0 = 2$ and $k = 4$. The continuous curve is the 'exact solution' of Kanoglu & Synolakis (2006), the broken curve is obtained using the conditions at $\lambda = 0$. The conditions at $\lambda = 0$ were obtained using an extrapolation based on the initial model given in (2.23).

the condition on that curve, rather than strictly at $\lambda = 0$; this can be seen in their equation (2.6) for φ which reads

$$\varphi(\sigma,\lambda) = \int_0^\infty [\varphi(\xi,\lambda_0(t=0))G_\lambda + \varphi_\lambda(\xi,\lambda_0(t=0))G]\,\mathrm{d}\xi. \tag{2.22}$$

Note that there is a factor of 2 in this expression in Kanoglu & Synolakis (2006), but we implicitly include this factor within G. We will show in appendix B that this expression derived by Kanoglu & Synolakis (2006) is the leading term of an asymptotic series. The second term in the asymptotic series is also computed in appendix B. According to appendix B these asymptotic series become meaningless for $\mathrm{d}\lambda_0/\mathrm{d}\xi > 1/2$.

The results that we obtain in this section concern mainly sources which are not extended in λ; therefore in order to have the condition at $\lambda = 0$, we make a very simple model of the very early stage of the evolution of the wave. Take an initial Gaussian waveform given by

$$\eta(t,x) \approx a\exp(-k\,(x - x_0 + \sqrt{x_0}t)^2) \tag{2.23}$$

where the centre of the Gaussian approaches the coast (without changing its shape) with a velocity of $\sqrt{x_0}$ during the very early stages of the wave propagation. Remember that for $\lambda = 0$, t is a function of σ only. The velocity of the fluid is approximately given by $-\eta/\sqrt{x}$. Using the simple evolution model given in (2.23), it is possible to derive the condition at $\lambda = 0$ at all σ. A comparison between the solution obtained this way and by the method presented by Kanoglu & Synolakis (2006) is given in figure 3.

2.3. *Test of the method using a discontinuous initial condition*

In this section we show that the particular Green's function method we adopt enables us to treat discontinuous initial conditions in space without any difficulty. As an

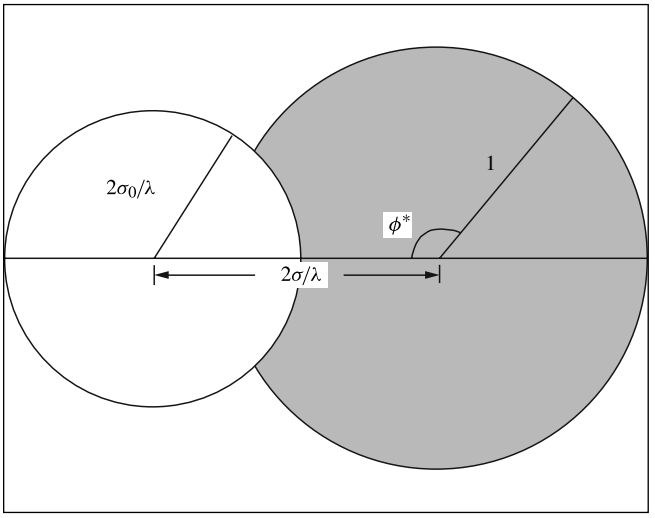

FIGURE 4. The domain of integration for (2.15) becomes the shaded area when the initial perturbation is $\eta(\sigma, \lambda = 0) = \eta_{max}\theta(\sigma - \sigma_0)$.

example case we considered a step-function-like initial condition of the following form on the slope:

$$\theta(\sigma - \sigma_0) \tag{2.24}$$

where θ is the step function. Note that for this kind of discontinuous forcing our domain of integration becomes the shaded area in figure 4. This domain excludes the region where the forcing is zero when evaluating the integral (2.15) which treats sources that are not extended in time. In the integral (2.15), when h becomes a step-function, the σ^* integral can be evaluated analytically. The results for various λ values are shown in figure 5.

2.4. *Landslide tsunami*

Although there are several analytical and numerical models for landslide tsunamis, there are fewer works in the run-up context, especially analytical and semi-analytical. One interesting study is Liu *et al.* (2003) in which the authors look at the landslide tsunami run-up problem within the framework of linearized shallow-water equations. Even though their study does not involve the CG approach, if we ignore the nonlinearity introduced by the right-hand side of (2.7) and replace it with a function of $\sigma - \lambda/2$, an analytical solution can be found by the linearized technique introduced by Liu *et al.* (2003). The linearized version of (2.7) for particular tsunamigenic forcing reads

$$\varphi_{\lambda\lambda} - \frac{1}{4\sigma}\varphi_\sigma - \frac{\varphi_{\sigma\sigma}}{4} = \partial_\lambda h(\sigma - \lambda/2). \tag{2.25}$$

The particular solution, φ_p, of this equation is given by

$$\varphi_p = -\tfrac{2}{3}(H(\sigma - \lambda/2) - \sigma h(\sigma - \lambda/2)) \tag{2.26}$$

where $H(\sigma - \lambda/2) = -\int_{\sigma-\lambda/2}^{+\infty} h(\sigma')\,\mathrm{d}\sigma'$. Liu *et al.* (2003) then proceed to add a solution of the homogeneous problem in order to satisfy the free-surface deformation and fluid velocity initial conditions (both to be zero).

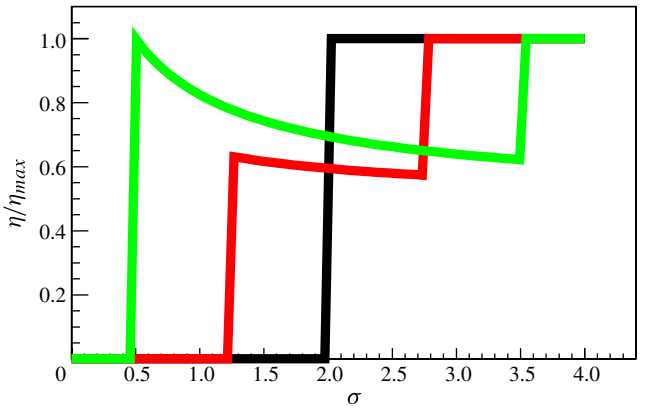

FIGURE 5. The evolution of the waveform at $\lambda = 0$, 1.5 and 3 is displayed as a function of σ (see (2.24)). The colour progression is black ($\lambda = 0$), red ($\lambda = 1.5$) and green ($\lambda = 3$). The initial shape is given by $\eta_{max}\theta(\sigma - \sigma_0)$ with $\sigma_0 = 2$ and $\eta_{max} = 10^{-6}$. The initial velocity is zero. The wave height is normalized to η_{max}.

However, if one assumes the forcing to be a function of $\sigma - \lambda/2$, this would correspond to the unphysical situation where the landslide having a density twice that of the water starts its motion at the shoreline and continues to move unopposed towards the deep basin, with a velocity proportional to the square root of the distance to the shoreline. Such an approach, despite the unphysical acceleration model of the sliding motion, is important in the sense that it sets an upper bound for the wave heights for this kind of phenomenon. We can reproduce the analytical result of Liu *et al.* (2003) by numerically evaluating the integrals given in (2.14), see asterisks and circles in figure 6 for our matching using the integral method.

In this work, our aim is to combine the integral method developed in the previous section with the forcing by a landslide that moves according to the following equation (see Watts 2000):

$$x_b'(t') = \frac{v'^2_\infty}{a'_{in}} \ln\left(\cosh\left(\frac{a'_{in}t'}{v'_\infty}\right)\right) + x'_{in} \tag{2.27}$$

where $v'_\infty = \sqrt{(2\alpha m/c_d A\rho_w)(\rho_b - \rho_w)g}$ is the terminal velocity, c_d is the drag coefficient, α is the slope and m is the mass of the sliding block, ρ_b and ρ_w are the densities of the sliding block and water and $a'_{in} = g\alpha(\rho_b - \rho_w)/\rho_w$ is the initial acceleration. The linearized source term in (2.7) will then be $J(\partial/\partial t)h \approx -v_b(\partial h/\partial x) \approx -v_b 2\sigma(\partial h/\partial\sigma)$ where v_b is the dimensionless velocity of the sliding block. Here we use a simple representation of the motion of the landslide with respect to a fixed frame of reference. For the landslide moving on the slanted bottom, we thus have

$$h(x, t) = h\left(x - \int_0^t v_b(\tilde{t})\,\mathrm{d}\tilde{t}\right). \tag{2.28}$$

An alternative approach to the problem of a sliding block could be to expand φ in terms of Bessel functions (see Aydin & Kanoglu 2007):

$$\varphi = \sum_{n=-N, n\neq 0}^{N} a_n(\lambda) J_0^*\left(\frac{\beta_{|n|}}{D}\sigma\right) \exp\left(\mathrm{i}\frac{\beta_{|n|}}{2D}\mathrm{sgn}(n)\lambda\right) \tag{2.29}$$

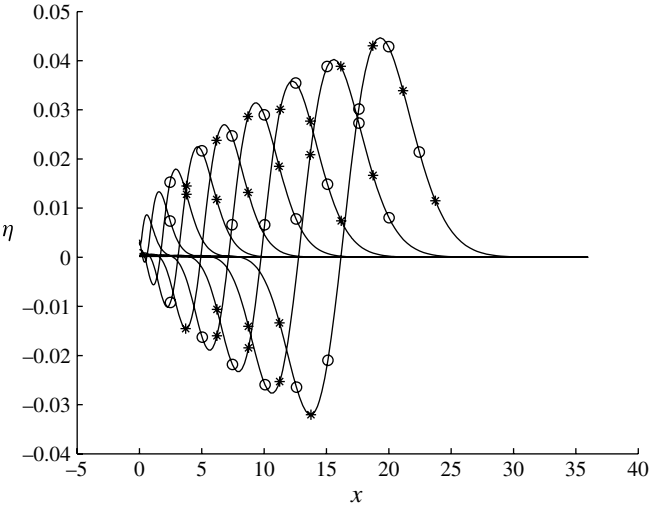

FIGURE 6. The results displayed in this figure are solutions of the linearized version of (2.7) where the right-hand side has been replaced by the derivative of $h(\lambda, \sigma) = a\exp(-k(\sigma - \lambda/2)^2)$ with respect to λ. We take a and k to be equal to 0.017 and 4 respectively. Note that (2.7) is very similar to (1.1) of Liu *et al.* (2003). These solutions are obtained by three different techniques. (i) The asterisks are the solution obtained by adding the homogeneous solution of (2.25) to the particular solution given in (2.26) in order to have η and the velocity both vanishing for $\lambda = 0$ (not $t = 0$). This is essentially equivalent to the technique of Liu *et al.* (2003) who worked in the (x, t) space. (ii) The circles are the solution obtained using the integral given in (2.14). (iii) Finally, the continuous curve is obtained by numerically solving the systems of ordinary differential equations (2.33) and (2.34).

where β_k is the kth root of Bessel function J_0 and sgn denotes the signum function. Here $J_0^*((\beta_{|n|}/D)\sigma)$ is the Bessel function with the unconventional normalization of

$$\int_0^D \mathrm{d}\sigma\,\sigma J_0^*\left(\frac{\beta_{\langle n\rangle}}{D}\sigma\right) J_0^*\left(\frac{\beta_{\langle n\rangle}}{D}\sigma\right) = 1. \tag{2.30}$$

For convenience of numerical calculation, a reflecting boundary is introduced at $\sigma = D$. When the waves reach $\sigma = D$, the model becomes unphysical. Because of the activity of the source S during the *time* interval $\mathrm{d}\tilde{\lambda}$, the quantity φ will change by an amount given by

$$\mathrm{d}\varphi = \mathrm{d}\tilde{\lambda}\sum_{n>0}\frac{2D}{\beta_n}\left(\int \mathrm{d}\tilde{\sigma}\,\tilde{\sigma}J_0^*\left(\frac{\beta_n\tilde{\sigma}}{D}\right)S(\tilde{\sigma},\tilde{\lambda})\right)J_0^*\left(\frac{\beta_n\sigma}{D}\right)\sin\left(\frac{\beta_n(\lambda-\tilde{\lambda})}{2D}\right). \tag{2.31}$$

This is so, because for a distribution of sources acting for an infinitesimal 'duration' $\mathrm{d}\tilde{\lambda}$ the retarded response is given simply by

$$\mathrm{d}\varphi(\sigma,\lambda) = \left(\int \mathrm{d}\tilde{\sigma}\,\tilde{\sigma}S(\tilde{\sigma},\tilde{\lambda})G\right)\mathrm{d}\tilde{\lambda} \tag{2.32}$$

where G is the corresponding retarded Green's function which, in our case, is composed of the Bessel and trigonometric functions.

Equation (2.31) yields the following set of coupled ordinary differential equations for the coefficients $a_n(\tilde{\lambda})$:

$$\frac{\mathrm{d}a_n}{\mathrm{d}\tilde{\lambda}} = \sum_{n>0} \frac{D}{\mathrm{i}\beta_n} \left(\int \mathrm{d}\tilde{\sigma}\, \tilde{\sigma} J_0^* \left(\frac{\beta_n \tilde{\sigma}}{D} \right) S(\tilde{\sigma}, \tilde{\lambda}) \right) \exp\left(\mathrm{i} \frac{-\beta_n \tilde{\lambda}}{2D} \right) \tag{2.33}$$

for $n > 0$ and

$$\frac{\mathrm{d}a_n}{\mathrm{d}\tilde{\lambda}} = \sum_{n<0} \frac{D}{\mathrm{i}\beta_{|n|}} \left(\int \mathrm{d}\tilde{\sigma}\, \tilde{\sigma} J_0^* \left(\frac{\beta_{|n|} \tilde{\sigma}}{D} \right) S(\tilde{\sigma}, \tilde{\lambda}) \right) \exp\left(\mathrm{i} \frac{\beta_{|n|} \tilde{\lambda}}{2D} \right) \tag{2.34}$$

for $n < 0$.

If one does not linearize the sources, the source distribution becomes a function of φ so that the right-hand sides of (2.33) and (2.34) depend on the coefficients a_n, leading to a set of coupled nonlinear ordinary differential equations. Solving the set of ordinary differential equations is the most general method as it does not involve any linearization other than omitting the term $[uh_x]_x$ in (2.1).

Returning to the linear case where forcing is given by $\partial_\lambda h(\sigma - \lambda/2)$, the solution of (2.25) computed by the three different methods is displayed in figure 6. These three approaches are basically: (i) the integration of the retarded Green's function by solving the set of ordinary linear differential equations (2.33) and (2.34); (ii) the analytical results obtained by adding the homogeneous solution to the particular solution (2.25) (for a very similar treatment in the (x, t) space see Liu *et al.* 2003) and (iii) the integral approach introduced by (2.14). A good match between these three methods can be observed.

3. Application to accelerating landslides

As an application we looked at the run-down and run-up created by a Gaussian-shaped landslide moving down obeying (2.27). Figure 7 shows the non-dimensional run-down and run-up of the shoreline for two cases of landslides with identical starting positions but with different thicknesses. The first impression is that the run-down is much more prominent than the run-up for both cases. This is because the negative source (the rear of the landslide) is closer to the shore while the positive source positioned at the front of the landslide creates a free-surface displacement that becomes smeared during its longer course towards the coast. Figure 7 superimposes results calculated with two different techniques discussed in this work, namely the set of ordinary differential equations (2.33), (2.34) and the integral solution given in (2.14). For both cases the solutions with these two techniques match almost perfectly. It is observed that the maximum run-down for both cases occurs at the non-dimensional time $t \approx 2$ and the time to reach the shore for the wave created at the initial movement of the landslide is $2\sqrt{x_0(0)}$ where $x_0(0)$ is the initial position of the centre of the Gaussian-shaped landslide. In this particular case $x_0(0) = 1$ which means that the maximum occurrences of run-down were created at the very early stage of the slide. The main reason the two techniques produce almost identical results is that at the instance the initial wave causing the maximum run-down is created, the Jacobian is close to unity (see figure 8). We also ran a series of tests with slides starting from various distances to the shoreline. In these tests we kept the landslide thickness and shape fixed. The two techniques gave almost identical results except in one case where the landslide starts its motion very close to the shoreline (figure 9*d*). For the starting position $x_0 = 0.25$ the integral approach gives slightly larger values of run-down and

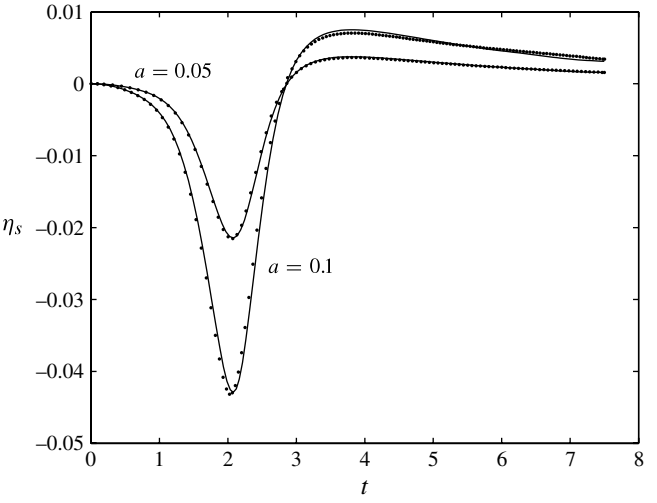

FIGURE 7. The run-down and run-up η_s as a function of t. The initial position of the centre is at 1000 m from undisturbed shoreline and the shape of the Gaussian landslide is given by $h(t, x) = a \exp(-4\,(x - x_0(t))^2)$. The initial value of non-dimensional x_0 is 1, the scale L is 1000 m. The landslide amplitude a takes the values of 0.05 and 0.1 for the plots given in this figure. The hydrodynamic friction coefficient $c_D = 1$ and slope α is 0.05. The density of the sliding material is 2000 kg m^{-3}. The diamonds are the solution calculated using (2.33), (2.34) and the continuous curve corresponds to the integral solution given in (2.14).

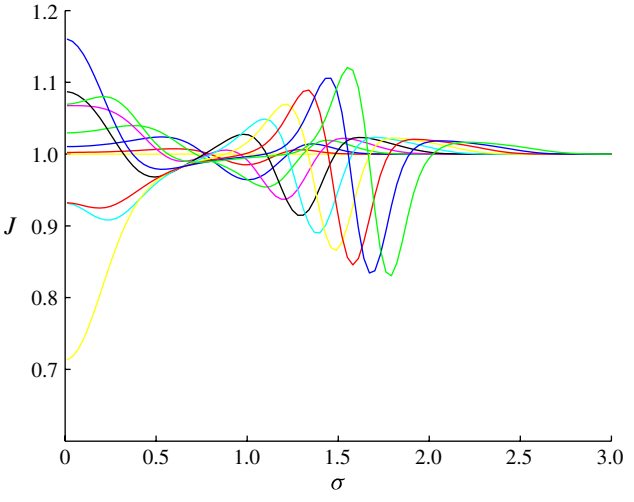

FIGURE 8. The Jacobian in (2.7) as a function of σ for $\lambda = 0,\ 0.3,\ 0.6, \ldots, 3.0$, corresponding to the colour progression yellow, red, blue, green, magenta, black, cyan, yellow, red, blue, green, respectively. The maximum thickness a of the sliding material is 0.05. All other parameters of the landslide are identical to those in figure 7.

run-up. The reason for these mismatches is the Jacobian, which is not taken into account in the integral approach.

The way that Carrier *et al.* (2003) non-dimesionalize the coordinates before the transformation renders the problem essentially independent of the slope α. If one

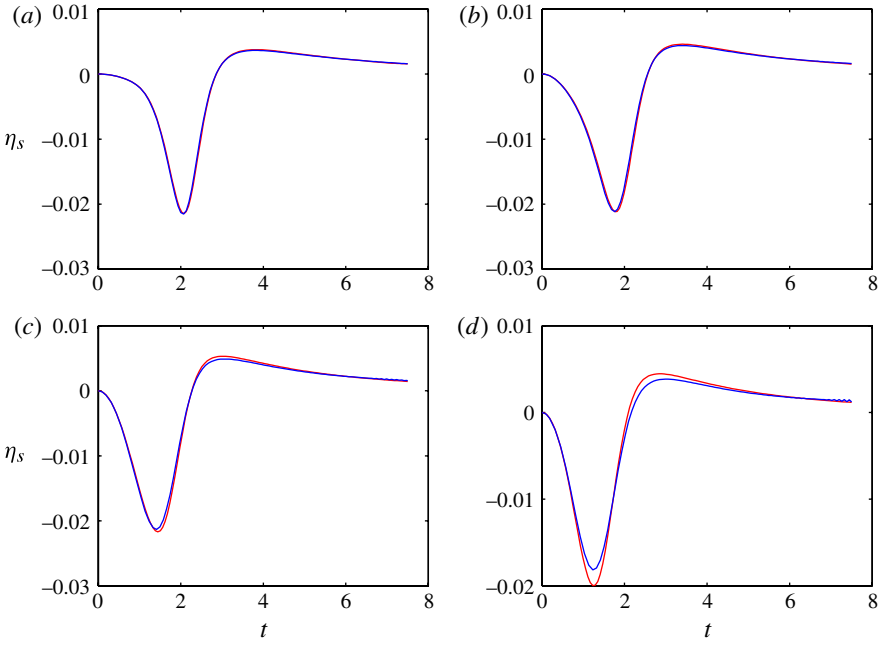

FIGURE 9. Run-down and run-up as a function of time for different values for the initial distance between the midpoint of the sliding block and the shoreline. The red curves are obtained using the integral method given by the (2.19) and blue curves are obtained by solving the system of ordinary differential equations given in (2.33) and (2.34). The form of the landslide is given by $h(x,t) = a\exp(-k\,(x - x_0(t))^2)$ where we took $k = 4$ and $a = 0.01$. (*a*), (*b*), (*c*) and (*d*) correspond to initial distances (x_0) of 1, 0.75, 0.5 and 0.25 respectively. The parameters L, ρ_b, c_D, k, $x_0(t = 0)$ and α are the same as those in figure 7.

ignores the hydrodynamic and basal frictions, then the acceleration of the block also scales with αg which makes the final solution also independent of α. If one takes the hydrodynamic friction into account, then the problem changes its nature because the hydrodynamic friction does not scale with αg, but in practice this has very little influence on the maximum run-down because the hydrodynamic drag effects start to be non-negligible only at the later stages of the landslide motion.

Liu *et al.* (2003) treated the landslide kinematics in an artificial way in which the landslide moves down with a velocity equal to $\sqrt{x}$. In their work there is a perfect coupling between the landslide motion and the wave field. In figure 10 we show the landslide movement and the wave field evolution as snapshots for the case in which we calculated the landslide motion taking the hydrodynamic friction into account. In this example the landslide starts its motion at $x = 1$. Figure 10 shows that the waveform extends during its evolution and the landslide lags behind the wave front. As seen in the figure, the negative peak starts to have a distorted shape. These shape effects exist because the wave propagation velocity depends on the position.

4. Comparison with a laboratory experiment

Although there are several landslide tsunami experiments in the literature (see for example Watts 2000; Liu *et al.* 2005; DiRisio *et al.* 2009) none of them examined the run-up in two dimensions. Hence, the comparison of our analysis with the laboratory experiments has limitations due to the fact that the sliding mass in all published run-up

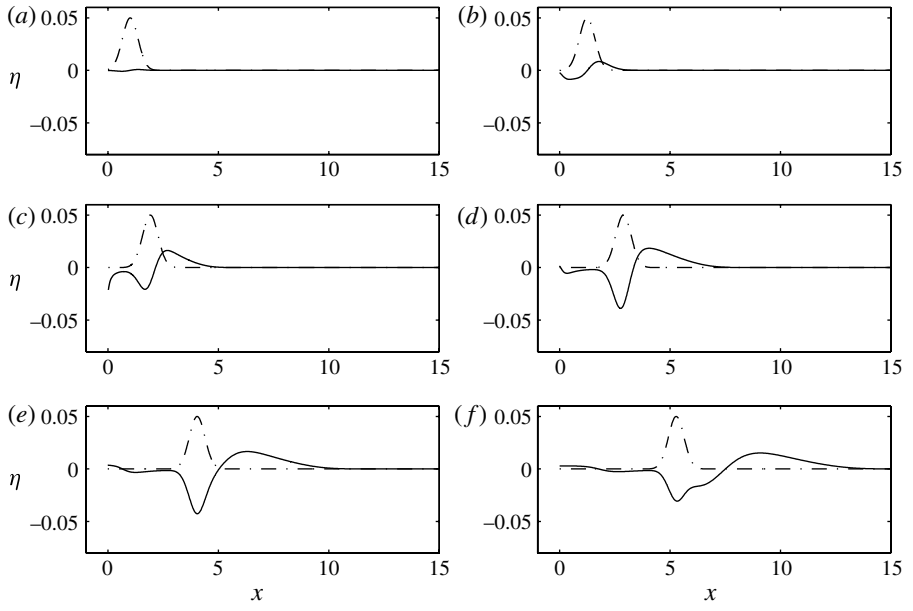

FIGURE 10. Snapshots of both the wave (continuous curve) and the landslide (broken curve) at non-dimensional times of $t = 0.2(a), 1(b), 2(c), 3(d), 4(e), 5(f)$. The values are calculated for a landslide shape given by $h(t, x) = a\exp(-k\,(x - x_0(t))^2)$ with $a = 0.05, k = 4$. The initial value of non-dimensional x_0 is 1, the scale L is 1000 m. The hydrodynamic friction coefficient $c_D = 1$ and slope α is 0.05. The density of the sliding material is 2000 kg m^{-3}.

experiments starts too close to the shoreline thus violating the assumptions needed in the theoretical CG treatment, or they start too far from the shore resulting in three-dimensional effects, which are also not possible in the CG treatment. For comparison purposes we selected Liu *et al.* (2005) because despite being a three-dimensional study, they conducted their experiments with particular attention to measuring run-up. Liu *et al.* (2005) did their experiments in a large hydraulic channel that has a length 104 m, width 3.7 m and depth 4.6 m. We do our comparisons for a specific experiment in which they used a right-triangle-shaped block to represent the landslide. We used (2.27) to calculate the landslide motion but the initial acceleration and the terminal velocity have been modified to take into account the Coulomb friction (see table 1 in Liu *et al.* 2005); we took the hydrodynamic drag coefficient c_d to be equal to 1. The mathematical representation of the moving triangular block to represent the landslide requires the use of a source and sink distribution given by $\partial h'/\partial t'$ where h' is the local value of the dimensional thickness of the landslide. If the block is rigid, we have $\partial h'/\partial t' = -v_b(\partial h'/\partial x')$ where v_b is the velocity of the block. The spatial derivative of the thickness presents a discontinuity in the case of a triangular block. The consequence of this is excitation of waves with wavelengths much shorter than the water depth. In this limit the shallow-water approximation is no longer valid.

In the linearized theories (for both shallow water and fully dispersive, linearized deep water), the deformation of the free surface during the time interval dt can be split into two parts. The first part is due to the progression of the wave generated prior to the interval dt. The second part is associated with the uplift or subsidence of the sea bottom during dt. We evaluate this second contribution using potential theory in which no assumption is made on the wavelengths. In potential theory, if an impulsive source

acts within a water body, the free-surface response can be expressed as the linear summation of an impulsive and non-impulsive terms (see the first line of equation (6) of Postacioglu & Özeren 2008). In this formalism even the solid block movements that are parallel to the sea bottom can be expressed in terms of series of instantaneous uplifts and subsidences. In the shallow-water approximation the impulsive responses of the free surface to these impulsive uplifts and subsidences are geometrically identical to the bottom motions. However, we calculate the initial generation of the waves created in the laboratory experiment by the triangular block using potential theory in which the waves created by short-wavelength features such as the corners of the triangular block are smeared out. Correcting the generation process of the waves for finite depth, (2.7) becomes

$$\varphi_{\lambda\lambda} - \frac{1}{4\sigma}\varphi_{\sigma} - \frac{\varphi_{\sigma\sigma}}{2} \approx \int_0^{\infty} \mathrm{d}\tilde{x} Q_{\lambda}(\lambda, \tilde{x}) \eta_{im}(x, \tilde{x}) \tag{4.1}$$

where $\eta_{im}(x, \tilde{x})$ is the impulsive response of the free surface to a unit volume input at $x = \tilde{x}$. Here x is assumed to be equal to σ^2. In this equation, Q_{λ} is the rate of fluid input and it is equal to $-v_b h_x$. The impulsive response is obtained by solving the Laplace equation in two dimensions (Miloh, Tyvand & Zilman 2002). The velocity potential $\phi_{im}(x, y)$ associated with the impulsive response satisfies the boundary conditions $\partial_n \phi_{im} = \delta(x - \tilde{x})$ at the bottom and $\phi_{im} = 0$ at the undisturbed free surface. When the total response (including to impulsive volume input at $t = \tilde{t}$) is considered, the associated velocity potential ϕ satisfies (see equation (6) in Postacioglu & Özeren 2008)

$$\lim_{t \to \tilde{t}^{+}} \phi = 0. \tag{4.2}$$

According to (4.2) the impulsive volume injections do not immediately affect the depth-averaged horizontal velocity. Consequently these volume injections do not create impulsive changes in the linear momentum balance.

To solve the Laplace equation in a wedge-like region we proceed to a conformal mapping (Tyvand & Storhaug 2000). In order to simulate the experiment of Liu *et al.* (2005) we take the slope angle to be equal to 26.56°. We map the wedge-like region onto the fourth quadrant of the complex plane using the transformation given by $z^{90°/26.56°}$ where $z = 0$ corresponds to the shoreline and the positive real axis is the undisturbed free surface. The negative imaginary axis is the sea bottom. We consider a series of infinite line sources perpendicular to the vertical plane to represent the landslide motion in the essentially three-dimensional experiment by Liu *et al.* (2005). These sources map onto the negative imaginary axis under the conformal transformation mentioned above. In the transformed space we also have to consider the images of these sources with respect to the undisturbed free surface to satisfy the zero-pressure condition at the free surface. Since, in the transformed space, the sources and their images are both on the imaginary axis the no-flux condition at the sea bottom is not violated by the images. We calculate the right-hand side of (4.1) using this conformal mapping.

Table 1 shows a comparison between our results and the experimental results of Liu *et al.* (2005). Note that the symbol R' in table 1 denotes the dimensional vertical displacement of the shoreline (see figure 4 of Liu *et al.* 2005); the experimental values have been taken from their figure 10.

When the vertical side of the triangular block is larger than the initial immersion, our analytical model underestimates the run-up. This is due to the fact that in

Init. immersion (cm)	−49.4	−39.5	−29.4	−20.2	−13.0	−9.7	−4.3
Analytical R' (cm)	0.9	1.05	1.25	1.5	1.9	1.97	2.34
Experimental R' (cm)	0.44	0.89	1.4	1.8	1.7	2.4	3.1

TABLE 1. Comparisons with experiments. R' indicates the vertical displacement of the shoreline. The Coulomb friction is taken to be 0.1482 (see table 10 of Liu *et al.* 2005, serie-B), and the mass of the sliding block to be 355.9 kg.

obtaining (2.6) we neglected the term $(uh)_x$ in (2.1). In reality the flow towards the shore above the block is confined to the narrow region between the top of the block and the free surface; however our formulation assumes that the thickness of the block is much smaller than the water depth, therefore underestimating the flow velocities, and hence the run-up. For intermediate initial depths the analytical model matches the experimental data better; however the error that stems from not taking the geometrical spreading effects into account may cancel some of the errors associated with distortion of the bathymetry by the block as mentioned above. For deeper initial immersions the two-dimensional analytical theory tends to overestimate the run-up possibly because of the geometrical spreading of the wave field which cannot be taken into account in the CG formalism.

Note that Sammarco & Renzi (2008) also compared their results with a three-dimensional experiment. They were particularly interested in waves trapped along the shore. Their formulation is also a shallow-water formulation without CG treatment while including an extra dimension along the shore. They interpret their overestimation of the laboratory results as due to the fact that their model does not take into account energy dissipation phenomena. We do not agree with their interpretation because the experiment they use is at the limit of shallow-water approximation, with the width of the block being comparable to the maximum depth the block reaches by the time it is completely submerged (about 24 cm). In fully dispersive deep water, disturbances with wavelength λ occurring at the bottom are reduced by the factor $\exp(-2\pi D/\lambda)$, where D is the water depth. Shallow-water theory cannot account for this reduction; thus it tends to overestimate the small-wavelength features.

5. Conclusion

In this work we have developed a novel integral approach that enables us to model run-down and run-up due to tsunami sources that are extended both in time and space. This particular approach is capable of modelling run-down and run-up of the tsunami waves created by landslides with a variety of kinematic structures. The Green's function that Kanoglu & Synolakis (2006) used is the same as that used in Carrier *et al.* (2003). However, Kanoglu & Synolakis (2006) surmounted the difficulty in evaluating the integrals involving G_λ by cutting out short-wavelength contributions to the Green's function. One strength of this new formulation is that there is no longer the need of numerical differentiation of the convolution of the Green's function with the source (Carrier *et al.* 2003, equation (27)) with respect to time-like variable λ. Instead, we analytically differentiate the source. Another advantage of the formulation is that it is numerically more stable than the methods such as that of Kanoglu (2004) for small-wavelength bottom deformations, making it more appropriate for landslide tsunamis where the tsunami source is very localized. Equation (2.16) is mathematically simple and it does not require any particular behaviour for initial η as opposed to

equation (2.9) of Kanoglu (2004) which includes a non-integrable singular term if the initial η has non-vanishing derivatives with respect to σ.

Acknowledgements

We would like to thank Air Lieutenant-General (retired) Ş. Dingiloğlu for encouraging us to undertake tsunami research.

Appendix A. Treatment of zero-velocity initial condition using Legendre polynomials

In this appendix, we show that the solution of initial-value problem developed by Tinti & Tonini (2005) can be expressed in series in terms of Legendre polynomials. Consider the Laplace equation in cylindrical coordinates:

$$\left(\partial_{zz} + \frac{1}{\sigma}\partial_{\sigma} + \partial_{\sigma\sigma}\right) f = 0. \tag{A 1}$$

The solution to this equation in terms of Legendre polynomials reads

$$f = \frac{1}{\left(\sigma^2 + z^2\right)^{(n+1)/2}} P_n\left(\frac{z}{\sqrt{\sigma^2 + z^2}}\right). \tag{A 2}$$

If we now introduce a transformation given by $z = 1 + \mathrm{i}\lambda/2$ where $\mathrm{i} = \sqrt{-1}$, the Laplace equation becomes the homogeneous version of (2.7) and both real and imaginary parts of

$$\frac{1}{\left(\sigma^2 + (1 + \mathrm{i}\lambda/2)^2\right)^{(n+1)/2}} P_n\left(\frac{1 + \mathrm{i}\lambda/2}{\sqrt{\sigma^2 + (1 + \mathrm{i}\lambda/2)^2}}\right) \tag{A 3}$$

are solutions of this equation. Furthermore, the imaginary part vanishes uniformly at $\lambda = 0$. Thus the imaginary part can be used to look at the evolution of initial waveforms with zero initial velocities. This approach is somewhat simpler than the calculations starting from equation (3.20) of Tinti & Tonini (2005)

Appendix B. Asymptotic expansion for the incident wave

In this appendix we will show that the integral

$$\int_0^{\infty} [\varphi(\xi, \lambda_0(\xi)) G_{\lambda}(\sigma, \xi, \lambda - \lambda_0(\xi)) + \varphi_{\lambda}(\xi, \lambda_0(\xi)) G(\sigma, \xi, \lambda - \lambda_0(\xi))]\, \mathrm{d}\xi \tag{B 1}$$

in the limit $\lambda \to \lambda_0(\sigma)^+$ reduces to

$$\frac{1}{2}\left(\frac{1}{1 + \frac{1}{2}\frac{\mathrm{d}\lambda_0}{\mathrm{d}\xi}\Big|_{\xi=\sigma}} + \frac{1}{1 - \frac{1}{2}\frac{\mathrm{d}\lambda_0}{\mathrm{d}\xi}\Big|_{\xi=\sigma}}\right) \varphi(\sigma, \lambda_0(\sigma)) \tag{B 2}$$

provided that $\mathrm{d}\lambda/\mathrm{d}\xi < 2$. If this condition is not satisfied, then the characteristic cones of the waves excited on the curve $\lambda_0(\xi)$ touch the curve again for larger values of λ,

which makes it impossible to obtain a closed form of the integral given in (B 1) in the limit $\lambda \to \lambda_0\,(\sigma)^+$. This is not an important problem in practice because the usual values of $\mathrm{d}\lambda_0/\mathrm{d}\xi|_{\xi=\sigma}$ are much smaller than 1. The major contribution to the integral given in (B 1) in the limit $\lambda \to \lambda_0\,(\sigma)^+$ comes from the vicinity of σ. The derivative of the Green's function given in Kanoglu & Synolakis (2006) with respect to λ is

$$G_\lambda(\xi, \sigma, \lambda - \lambda_0(\xi)) = \xi \int_0^\infty \omega J_0(\omega\xi) J_0(\omega\sigma) \cos\left(\tfrac{1}{2}\omega(\lambda - \lambda_0(\xi))\right) \mathrm{d}\omega. \tag{B 3}$$

In the region of interest, the argument of the cosine function in the integrant of (B 3) may be approximated by $(\omega/2)(\mathrm{d}\lambda_0/\mathrm{d}\xi)|_{\xi=\sigma}(\xi - \sigma)$. Carrying out the integration (B 1) with this approximation we obtain (B 2) So, in order to have a slightly better approximation for both φ and φ_λ initial conditions, it suffices to express φ as

$$\varphi \approx 2 \int_0^\infty \left[\frac{1}{1 + \frac{1}{2}\dfrac{\mathrm{d}\lambda_0(\xi)}{\mathrm{d}\xi}} + \frac{1}{1 - \frac{1}{2}\dfrac{\mathrm{d}\lambda_0(\xi)}{\mathrm{d}\xi}} \right]^{-1} (\varphi(\xi, \lambda_0) G_\lambda + \varphi_\lambda(\xi, \lambda_0) G)\, \mathrm{d}\xi. \tag{B 4}$$

In order to show the slight accuracy gain by the use of (B 4) we consider an incident wave of the following form:

$$\eta = a\sigma^3 \exp(-k\,(\sigma^2 - \sigma_0^2)^2). \tag{B 5}$$

The introduction of the σ^3 factor in this formulation of η has a special purpose. For incident waves, u_0 (the fluid velocity at $t = 0$) is approximately given as $-\eta/\sqrt{x}$. The σ^3 factor ensures that the derivative of u_0 with respect to σ at $\sigma = 0$ vanishes. Bessel functions of order zero have the same property so that the expansion of u_0 in terms of Bessel functions does not lead to spurious oscillations

We wish to calculate u in the following limit:

$$\lim_{\lambda \to \lambda_0(\sigma)} u = u_0 \tag{B 6}$$

using (B 4) and equation (4) of Kanoglu & Synolakis (2006) separately. table 2 compares the u_0 values calculated using these two approaches for various values of a and σ (we take $\sigma_0 = 0.3$ and $k = 2$). All results shown in the table are normalized by u_0.

As seen from table 2, the differences between the two approaches are too small to represent using a curve, nevertheless (B 4) performs better.

Appendix C. Computational load of the integral approach

Here we briefly summarize the computational load involved in the new integral approach proposed in this manuscript. To evaluate the σ^* integral in (2.14) we used 20 points (see table 3). For the angular (ϕ^*) integral we used between 64 and 256 points depending on the thickness of the sliding mass. When we use 256 points for the angular integration in (2.14) the $\sigma^* - \phi^*$ double integration takes 4 ms on an AMD-P960 processor with clock speed of 1.8 GHz using single core. For the run-up case ϕ^* the integral can be carried out analytically. For the solutions of the system of ordinary differential equations given in (2.32) and (2.33) we used standard numerical

a	σ	Kanoglu & Synolakis (2006)	(B 4)
0.017	0.35	1.00003069881609	1.00000000093789
0.017	0.4	1.00001201741069	1.00000000004529
0.017	0.45	1.00000000022340	1.00000000018732
0.017	0.50	1.00002490033332	1.00000000035723
0.017	0.55	1.00013226950913	1.00000001781832
0.017	0.60	1.00037006448834	1.00000013646232
0.085	0.35	1.00076488804027	0.999997443048229
0.085	0.4	1.00030381141661	1.00000337626733
0.085	0.45	0.999996534912367	0.999996534010384
0.085	0.50	1.00062640076710	1.00000389893801
0.085	0.55	1.00331414196627	1.00000782388693
0.085	0.60	1.00933618289809	1.00008717727673
0.17	0.35	1.00342374387486	1.00035287281274
0.17	0.4	1.00080594858944	0.999604687111633
0.17	0.45	1.00044911535421	1.00044911174464
0.17	0.50	1.00205382364562	0.999564909412142
0.17	0.55	1.01364955152864	1.00041884340873
0.17	0.60	1.03881695955532	1.00175908840013

TABLE 2. Comparisons between the two different ways of reproducing u_0 using (B 4) and equation (4) of Kanoglu & Synolakis (2006).

Root	Weight
$3.485805338439398 \times 10^{-3}$	$8.935711915945818 \times 10^{-3}$
$1.827857775609691 \times 10^{-2}$	$2.060476871757802 \times 10^{-2}$
$4.453461199377553 \times 10^{-2}$	$3.184163121644321 \times 10^{-2}$
$8.165347784856671 \times 10^{-2}$	$4.242550369556703 \times 10^{-2}$
$1.287738420718438 \times 10^{-1}$	$5.220765514300643 \times 10^{-2}$
$1.847944660686142 \times 10^{-1}$	$6.110041534311562 \times 10^{-2}$
$2.483971552410312 \times 10^{-1}$	$6.907043633180596 \times 10^{-2}$
$3.180755742444288 \times 10^{-1}$	$7.612753242428937 \times 10^{-2}$
$3.921698219472685 \times 10^{-1}$	$8.231201761849634 \times 10^{-2}$
$4.689059297052046 \times 10^{-1}$	$8.768287608497138 \times 10^{-2}$
$5.464389748055695 \times 10^{-1}$	$9.230796623279897 \times 10^{-2}$
$6.228984119875632 \times 10^{-1}$	$9.625682556970285 \times 10^{-2}$
$6.964344355286450 \times 10^{-1}$	$9.959607063150137 \times 10^{-2}$
$7.652641517011232 \times 10^{-1}$	$1.023866880889365 \times 10^{-1}$
$8.277161131459963 \times 10^{-1}$	$1.046824177918935 \times 10^{-1}$
$8.822718752021044 \times 10^{-1}$	$1.065288965267589 \times 10^{-1}$
$9.276035860445434 \times 10^{-1}$	$1.079633983603853 \times 10^{-1}$
$9.626068270921805 \times 10^{-1}$	$1.090149286896876 \times 10^{-1}$
$9.864280267986831 \times 10^{-1}$	$1.097045706395120 \times 10^{-1}$
$9.984858364913605 \times 10^{-1}$	$1.100460157724997 \times 10^{-1}$

TABLE 3. The roots and weights used for the σ^* integral in (2.14).

solvers. The $\tilde{\sigma}$ integrals on the right-hand sides had to be evaluated for each basis function and for each integral we used 2000 points. Calculating snapshots for various times takes longer because of the need to invert the results from (λ, σ) to (x, t) space.

REFERENCES

AMPARO, G., SEGURA, J. & TEMME, N. 2007 *Numerical Methods for Special Functions. Society for Industrial and Applied Mathematics*, SIAM.

ASSIER-RZADKIEWICZ, S., HEINRICH, P., SABATIER, P. C., SAVOYE, B. & BOURILLET, J. F. 2000 Numerical modelling of a landslide-generated tsunami: the 1979 nice event. *Pageoph* **157**, 1707–1727.

AYDIN, B. & KANOGLU, U. 2007 Wind set-down relaxation. *CMES – Comput. Modell. Engng Sci.* **21**, 149–155.

BARDET, J. P., SYNOLAKIS, C. E., DAVIES, H. L., IMAMURA, F. & OKAL, E. A. 2003 Landslide tsunamis: recent findings and research directions. *Pure Appl. Geophys.* **160**, 1793–1809.

CARRIER, G. F. & GREENSPAN, H. P. 1958 Water waves of finite amplitude on a sloping beach. *J. Fluid Mech.* **4**, 97–109.

CARRIER, G. F., WU, T. T. & YEH, H. 2003 Run-up and draw-down on a plane beach. *J. Fluid Mech.* **475**, 79–99.

DIRISIO, M., BELLOTTI, G., PANIZZO, A. & DEGIROLAMO, P. 2009 Three-dimensional experiments on landslide generated waves at a sloping coast. *Coast. Engng* **56**, 659–671.

GEIST, E. L. 2000 Origin of the 17 July 1998 Papua New Guinea tsunami: earthquake or landslide? *Seismological Res. Lett.* **71**, 344–351.

GEIST, E. L., LYNETT, P. J. & CHAYTOR, J. D. 2009 Hydrodynamic modelling of tsunamis from the Currituck landslide. *Mar. Geol.* **264**, 41–52.

KANOGLU, U. 2004 Nonlinear evolution runup-rundown of long waves over sloping beach. *J. Fluid Mech.* **513**, 363–372.

KANOGLU, U. & SYNOLAKIS, C. 2006 Initial value problem solution of nonlinear shallow water-wave equations. *Phys. Rev. Lett.* **97**, 148501.

LIU, P. L.-F., LYNETT, P. & SYNOLAKIS, C. E. 2003 Analytical solutions for forced long waves on a sloping beach. *J. Fluid Mech.* **478**, 101–109.

LIU, P. L.-F., WU, T. R., RAICHLEN, R., SYNOLAKIS, C. E. & BORRERO, J. C. 2005 Runup and rundown generated by three-dimensional sliding masses. *J. Fluid Mech.* **536**, 107–144.

MADSEN, P. A. & SCHÄFFER, H. A. 2010 Analytical solutions for tsunami runup on a plane beach: single waves, n-waves and transient waves. *J. Fluid Mech.* **645**, 27–57.

MILOH, T., TYVAND, P. A. & ZILMAN, G. 2002 Green function for initial free-surface flows due to three-dimensional impulsive bottom deflection. *J. Engng Maths* **43**, 57–74.

ÖZEREN, M. S., CAGATAY, M. N., POSTACIOGLU, N., ŞENGÖR, A. M. C., GORUR, N. & ERIS, K. 2010 Mathematical modelling of a potential tsunami associated with a late glacial submarine landslide in the sea of marmara. *Geomarine Lett.* **30** (5), 523–539.

POSTACIOGLU, N. & ÖZEREN, M. S. 2008 A semi-spectral modelling of landslide tsunamis. *Geophys. J. Intl* **175**, 1–16.

PRITCHARD, D. & DICKINSON, L. 2007 The near-shore behaviour of shallow-water waves with localized initial conditions. *J. Fluid Mech.* **591**, 413–436.

SAMMARCO, P. & RENZI, E. 2008 Landslide tsunamis propagating along a plane beach. *J. Fluid Mech.* **598**, 107–119.

TINTI, S. & TONINI, R. 2005 Analytical evolution of tsunamis induced by near shore earthquake on constant slope ocean. *J. Fluid Mech.* **535**, 33–64.

TYVAND, P. A. & STORHAUG, A. R. F. 2000 Green functions for impulsive free-surface flows due to bottom deflections in two-dimensional topographies. *Phys. Fluids* **12**, 2819–2833.

WANG, Y., LIU, P. L. F. & MEI, C. C. 2011 Solid landslide generated waves. *J. Fluid Mech.* **675**, 529–539.

WARD, S. 2001 Landslide tsunami. *J. Geophys. Res.* **106**, 11201–11215.

WATTS, P. 2000 Tsunami features of solid block underwater landslides. *J. Waterways Port Coast. Ocean Engng* **126** (3), 144–152.

WATTS, P., GRILLI, S. T., KIRBY, J. T., FRYER, G. J. & TAPPIN, D. R. 2003 Landslide tsunami case studies using a boussinesq model and a fully nonlinear tsunami generation model. *Nat. Hazards Earth Syst. Sci.* **3**, 391–402.

WITHAM, G. B. 1974 *Linear and Nonlinear Waves*. Wiley-Interscience.